A Family of Hybrid Analog–Digital Beamforming Methods for Massive MIMO Systems

Shahar Stein Ioushua ⬡, *Student Member, IEEE*, and Yonina C. Eldar ⬡, *Fellow, IEEE*

Abstract—In massive MIMO systems, hybrid beamforming is an essential technique for exploiting the potential array gain without using a dedicated RF chain for each antenna. In this paper, we consider the data phase in massive MIMO communication, where the transmitter and receiver use fewer RF chains than antennas. We examine several different fully and partially connected schemes and consider the design of hybrid beamformers that minimize the estimation error in the data. For the hybrid precoder, we introduce a framework for approximating the optimal fully digital precoder with a feasible hybrid one. We exploit the fact that the fully digital precoder is unique only up to a unitary matrix and optimize over this matrix and the hybrid precoder alternately. Our alternating minimization of approximation gap (Alt-MaG) framework improves the performance over state-of-the-art methods with no substantial increase in complexity. In addition, we present a special case of Alt-MaG, minimal gap iterative quantization (MaGiQ), that results in low complexity and lower mean squared error (MSE) than other common methods, in the case of very few RF chains. MaGiQ is also shown to coincide with the optimal fully digital solution in some scenarios. For combiner design, we exploit the structure of the MSE objective and develop a greedy ratio trace maximization technique that achieves low MSE under various settings. All of our algorithms can be used with multiple hardware architectures.

Index Terms—Massive multiple-input multiple-output (MIMO), antenna arrays, hybrid beamforming, precoding, combining, cellular communication, alternating minimization, low-complexity, ratio-trace minimization.

I. INTRODUCTION

MASSIVE MIMO wireless systems have emerged as a leading candidate for 5G wireless access [1], [2]. Along with mmWave technologies, that were recently recognized as essential for coping with the spectrum crunch [3], it offers higher data rates and capacities than traditional MIMO systems. The use of large-scale antenna arrays at both the transmitter and receiver holds the potential for higher array gain than before. To exploit this gain, precoding and combining techniques are used.

S. S. Ioushua is with the Dept. of Electrical Engineering, Tel Aviv University, Tel Aviv 6997801, Israel (e-mail: steinioushua@mail.tau.ac.il).

Y. C. Eldar is with the Department of Mathematics and Computer Science, Weizmann Institute of Science, Rehovot 7610001, Israel (e-mail: yonina.eldar@weizmann.ac.il).

Traditionally implemented in the baseband (BB), these methods require a dedicated RF hardware per antenna. Unfortunately, when taking a massive number of antennas into account, this results in very high cost, as the RF components are expensive and have high power consumption, especially for mmWave technologies. Hence, it is desirable to design economical hardware that will utilize the potential gain from a large number of cheap antenna elements using a small number of expensive RF chains.

To achieve this goal, several hybrid analog-digital schemes have been suggested [4]–[15]. In hybrid precoding and combining, the operations are split between the digital and analog domains: at the transmitter side a low dimensional digital precoder operates on the transmitted signal at BB. An analog precoder then maps the small number of digital outputs to a large number of antennas, and the same is performed at the receiver side. Common analog architectures are based on analog phase shifters and switches. The specific schemes can vary according to the power and area budget. Two main families of architectures are the fully- and partially connected structures. Fully connected networks offer a mapping from each antenna to each RF chain and allow maximizing the precoding and combining gain. In the partially connected scheme, a reduced number of analog components is used. This degrades the achieved gain but offers lower power consumption and hardware complexity.

In the data phase of each coherence interval of the MIMO communication process, the transmitter sends multiple data streams to the receiver over the constant and known channel, using precoding techniques. At the receiver side, a combiner is used to estimate the data vector from the received signal at the antennas. The precoder and combiner are chosen to optimize some desired performance measure, such as estimation error or spectral efficiency of the system. Unlike the fully-digital case, when considering a hybrid beamformer, the precoder and combiner matrices cannot have arbitrary entries, but are constrained according to the specific hardware choice. For example, when using a phase shifter network at the analog side, only unimodular matrices for the analog beamformer are considered. The goal then is to optimize the performance measure over all pairs of digital and analog precoder matrices, which yields a non-convex difficult optimization problem.

A. Related Works

The majority of past works on hybrid beamforming considered the fully-connected phase shifter network. In [4], it was suggested to separate the joint precoder and combiner design

problem into two subproblems and solve each independently. Although this approach is sub-optimal, it greatly simplifies the difficult joint optimization problem. For the precoder, it was shown that minimizing the gap between the hybrid precoder and the optimal fully-digital one over all hybrid precoders, approximately leads to the maximization of the system's spectral efficiency. On the combiner side, minimizing the mean squared error (MSE) over all hybrid combiners was shown to be equivalent to minimizing the weighted approximation gap between the fully-digital combiner and the hybrid one, with the weights given by the received signal correlation. Methods for solving these approximation problems were suggested in [4]–[11], [13].

In [5] the authors considered a fully-connected phase shifter scheme and showed that for flat-fading channels, if the number of RF chains is twice the number of data streams, then a hybrid beamformer can achieve the performance of a fully-digital one. They then suggest a heuristic algorithm for precoder design that first calculates the optimal baseband precoder for a fixed analog precoder, and then obtains a local optimal analog precoder by an iterative algorithm. The works [4], [6], [7] considered precoder design and aimed at maximizing the system's spectral efficiency. They exploit the mmWave sparse multipath channel structure and deduce that the optimal fully-digital precoder is composed of a small sum of steering vectors. They then suggest a variant of the orthogonal matching pursuit (OMP) [16] algorithm to construct a feasible precoder that approximates the optimal one using a dictionary of steering vectors. This solution greatly reduces the problem complexity but results in a large performance gap from the optimal precoder due to restricting the space of possible precoder vectors to steering vectors.

Similar approaches were followed in [4], [8], [9] for the combiner design, under a MSE or spectral efficiency objective. In [10], the authors considered both rich and sparse scattering channels and showed that for the asymptotic case when the number of antennas goes to infinity, the channel singular vectors are unimodular, and the optimal hybrid beamformer is obtained by setting the phase shifters to the phases of these vectors. In [11], two algorithms were suggested to approximate the optimal fully-digital precoder with a feasible one. The first, MO-AltMin, is based on manifold optimization. In each iteration of the algorithm, it assumes a given digital precoder and develops a conjugate gradient method to find an analog precoder that is a local minimizer of the approximation gap from the fully-digital one. Next, the digital precoder is computed using a least squares solution. This method achieves good performance but suffers from high complexity and run time, and is only suitable for fully-connected phase shifter networks. The second approach is a low complexity algorithm that assumes the digital precoder to be a scaled unitary matrix and uses this assumption to produce an upper bound on the approximation gap, which is then minimized over all analog precoders. However, limiting the combiner to such a structure results in performance loss.

For the partially connected architecture, most of the existing works concentrated on fixed sub-arrays where each RF chain is connected to a predetermined sub-array. In [12], the authors suggested a low complexity codebook design producing a small dictionary of feasible precoding vectors, that are chosen based on the transmitted signal strength. They then exhaustively search over all possible combinations from the small dictionary to maximize the mutual information between the receiver and transmitter. This last step can result in a heavy computational load when the channel is not sparse. In [11], the authors consider disjoint sub-arrays and suggest an iterative method to approximate the optimal fully-digital precoder, which optimizes over the analog and digital combiners alternately. It is shown that for disjoint arrays, the analog precoder problem is separable in the antennas, and has a closed form solution. For the digital precoder, a semidefinite relaxation is suggested. However, this is both computationally heavy and unnecessary since a closed form solution for the digital combiner is available. This alternating minimization approach still results in large performance gap. Some less restrictive schemes were considered in [13], [14]. In [13], a double phase shifter with dynamic mapping is considered. The use of two phase shifters per antenna relaxes the unit modulo constraint that limits the previous solutions, but costs twice the power consumption, area and complexity. In [14], a dynamic sub-array approach is considered for orthogonal frequency-division multiplexing (OFDM), and a greedy algorithm to optimize the array partition based on the long-term channel characteristics is suggested. However, this method is relevant only for OFDM transmissions.

B. Contributions

Most of the above works use spectral efficiency as their performance metric. In this work, we consider the MSE of the transmitted data as our main performance criterion. We develop a general framework for hybrid beamforming, suitable for various channels and hardware: full and partial networks with different numbers of phase shifters and switches. We consider the data estimation problem in a single user massive MIMO system where both the receiver and transmitter are equipped with large antenna arrays and fewer RF chains than antennas. We assume a Bayesian model where the data and interference are both random, and aim at minimizing the MSE of the transmitted data from the low dimensional received digital signal at the receiver, over all hybrid precoders and combiners, assuming a fixed number of RF chains. Like previous works, we relax the difficult joint optimization to two separate problems in the precoder and combiner.

To design the precoder, we present a framework for approximating the optimal fully-digital precoder with a feasible hybrid one. Our alternating minimization of approximation gap (Alt-MaG) method, exploits the fact that there exists an infinite set of optimal precoders, which differ by a unitary matrix. We suggest optimizing over this matrix and the hybrid precoder alternately, to find the fully-digital solution that results in the smallest approximation gap from its hybrid decomposition. For the hybrid precoder optimization step, any of the previously suggested methods [4], [6]–[9], [11], [13] may be used, according to the hardware constraints. By optimizing over the unitary matrix as well, Alt-Mag achieves additional reduction in MSE compared to state-of-the-art algorithms, with no significant increase in complexity.

We then present a simple possible solution for the hybrid precoder optimization step, that results in a low complexity algorithm, termed minimal gap iterative quantization (MaGiQ). In each iteration of MaGiQ, the fully-digital solution is approximated using the analog precoder alone. This results in a closed form solution, given by a simple quantization function which depends on the hardware structure. We demonstrate in simulations that MaGiQ achieves lower MSE than other low complexity algorithms when using very few RF chains. In addition, in some specific cases, it coincides with the optimal fully-digital solution. We show that the Alt-Mag framework and the MaGiQ algorithm can also be used when considering the spectral efficiency metric, and demonstrate the algorithms performance using this objective.

Next, we apply MaGiQ for combiner design with mild adjustments. We then suggest an additional greedy ratio trace maximization (GRTM) algorithm that directly minimizes the estimation error using a suitable dictionary that is chosen according to the hardware scheme. In simulations, we demonstrate that GRTM enjoys good performance and short running time, especially when the number of RF chains increases.

To summarize, our main contributions are as follows:

- A new framework, Alt-MaG, for hybrid beamformer design that exploits the degree of freedom in the unitary matrix in the optimal unconstrained beamformer. Alt-Mag boosts the performance of existing hybrid beamformers and can be used with various performance criteria such as MSE and spectral efficiency.
- A simple low-complexity algorithm, MaGiQ, that fits the Alt-MaG framework and achieves lower MSE than other low complexity algorithms when using very few RF chains.
- A greedy framework for combiner design that directly minimizes the estimation error by solving a simple ratio-of-scalars problem for each combiner vector separately.
- A simple algorithm, GRTM, for solving the ratio-of-scalar problem using a suitable dictionary that is chosen according to the hardware scheme.

All of our algorithms fit various hardware constraints and channel structures.

C. Organization and Notation

The rest of this paper is organized as follows: In Section II we introduce the signal model and problem formulation, and review common combiner hardware schemes. In Section III we formulate the massive MIMO data estimation problem as an MSE minimization over the precoder and combiner. Sections IV and V consider the precoder and combiner design problems, respectively. In Section VI we evaluate the proposed algorithms using numerical experiments under different scenarios.

The following notations are used throughout the paper: bold-face upper-case X and lower-case x are used to denote matrices and vectors respectively, and non-bold letters x are scalars. The ith element in the jth column of X is $[X]_{ij}$. We let I denote the identity matrix of suitable size, X^T, X^* the transpose and conjugate-transpose of X respectively, $\mathbb{E}\{\cdot\}$ the expectation and $\|\cdot\|_p^2$, $\|\cdot\|_F^2$ the ℓ_p and Forbenius norms, respectively. The

determinant of X is $|X|$, its trace is $\mathrm{tr}(X)$, and $\mathcal{CN}(x, X)$ is the complex-Gaussian distribution with mean x and covariance matrix X. The real part of a variable is denoted as $\Re\{\cdot\}$, the phase as $\angle(\cdot)$, $\mathcal{R}(X)$ is the range space of X and P_X is the orthogonal projection onto $\mathcal{R}(X)$.

II. PROBLEM FORMULATION

A. Signal Model

Consider a single user massive MIMO system in which a transmitter with N_t antennas communicates N_s independent data streams using N_{RF}^t RF chains, $N_s \leq N_{RF}^t \leq N_t$, to a receiver equipped with N_r antennas and N_{RF}^r RF chains, $N_s \leq N_{RF}^r \leq N_r$. At the transmitter, the RF chains are followed by a network of switches and phase shifters that expands the N_{RF} digital outputs to N_t precoded analog signals which feed the transmit antennas. Similarly, at the receiver, the antennas are followed by a network of switches and phase shifters that feed the N_{RF}^r RF chains. The specific architecture of the analog hardware at each end can vary according to budget constraints. Some possible choices are presented in the next subsection. For simplicity, we assume $N_{RF}^t = N_{RF}^r = N_s$, which corresponds to the minimal possible number of chains, and hence the worst-case scenario.

The hybrid architecture enables the transmitter to apply a BB precoder $F_{BB} \in \mathbb{C}^{N_{RF}^t \times N_{RF}^t}$, followed by a RF precoder $F_{RF} \in \mathcal{F}^{N_t \times N_{RF}^t}$. The properties of the set $\mathcal{F}$ are determined by the specific hardware scheme in use. For example, in fully-connected phase shifter networks, $\mathcal{F}$ is the set of unimodular matrices. The transmitter obeys a total power constraint such that $\|F_{RF} F_{BB}\|_F^2 = N_s$.

The discrete-time $N_t \times 1$ transmitted signal can be written as

$$x = F_{RF} F_{BB} s, \quad (1)$$

with s the $N_s \times 1$ symbol vector. We assume, without loss of generality, that $s \sim \mathcal{CN}(0, I_{N_s})$. The signal is transmitted over a narrowband block-fading propagation channel such that the $N_r \times 1$ received analog signal vector y at the receiver's antennas is

$$y = \sqrt{p_r} H F_{RF} F_{BB} s + z, \quad (2)$$

where H is the $N_r \times N_t$ channel matrix, p_r is the received average power and z is an $N_r \times 1$ interference vector with zero mean and autocorrelation matrix $\mathbb{E}[zz^H] = R_z$. In general, z can represent either noise or an interfering signal. Here we mostly consider the case where z is noise. In Section V-C we present one scenario in which z is interference. We assume full channel state information (CSI), i.e. the matrix H is known. The interference correlation matrix R_z is also known and assumed to be full rank.

At the receiver, an analog combiner maps the N_r inputs to N_{RF}^r RF chains that are then processed at baseband using a digital combiner. This yields the signal

$$r = \sqrt{p_r} W_{BB}^* W_{RF}^* H F_{RF} F_{BB} s + W_{BB}^* W_{RF}^* z, \quad (3)$$

with $W_{RF} \in \mathcal{W}^{N_r \times N_{RF}^r}$ the analog combining matrix and W_{BB} the $N_{RF}^r \times N_{RF}^r$ digital combining matrix. The proper-

ties of the set $\mathcal{W}$ vary according to the specific analog hardware scheme.

We wish to design $\boldsymbol{W}_{RF}, \boldsymbol{W}_{BB}, \boldsymbol{F}_{RF}, \boldsymbol{F}_{BB}$ to minimize the estimation error of $\boldsymbol{s}$ from $\boldsymbol{r}$, under different hardware constraints, i.e different feasible sets $\mathcal{W}, \mathcal{F}$. Thus, we consider the problem

$$\min_{\boldsymbol{W}_{RF}, \boldsymbol{W}_{BB} \boldsymbol{F}_{RF}, \boldsymbol{F}_{BB}} \mathbb{E}\left[\|\boldsymbol{s} - \boldsymbol{W}_{BB}^* \boldsymbol{W}_{RF}^* \boldsymbol{y}\|_2^2\right]$$

$$\text{s.t.}: \quad \boldsymbol{F}_{RF} \in \mathcal{F}^{N_t \times N_{RF}^t}, \quad \|\boldsymbol{F}_{RF}\boldsymbol{F}_{BB}\|_F^2 \leq N_s,$$

$$\boldsymbol{W}_{RF} \in \mathcal{W}^{N_r \times N_{RF}^r}. \tag{4}$$

B. Precoder and Combiner Hardware Schemes

We now present some possible hardware schemes and the feasible sets they dictate. We focus on the combiner architecture and the feasible set $\mathcal{W}$, but all the options presented here can be translated to similar precoder networks and feasible sets $\mathcal{F}$. The networks below are based on phase shifters and/or switches, with different connectivity levels. In practice, the choice of scheme can be affected by a variety of budget constraints such as power consumption, price, and area against the requested array gain. For example, phase shifters allow for a more flexible design than switches, but their power consumption is higher.

S1) **Fully Connected Phase Shifters and Switches Network:** Each antenna is connected to an RF chain through an independent on/off switch followed by a phase shifter. All the incoming analog signals from the different antennas are combined before feeding the RF chain. In this architecture, the entries of the analog combining matrix $\boldsymbol{W}_{RF}$ can be either zeros or unit modulus. Hence the set $\mathcal{W}$ is defined by $\mathcal{W}^{N_r \times N_{RF}^r} = \{\boldsymbol{W} \in \mathbb{C}^{N_r \times N_{RF}^r} : |w_{ij}| \in \{0, 1\}\}$. The orthogonal projection $\boldsymbol{P}_{\mathcal{W}}$ onto the feasible set dictated by this scheme is defined as

$$[\boldsymbol{P}_{\mathcal{W}}(\boldsymbol{A})]_{il} = \begin{cases} e^{j2\pi\angle[\boldsymbol{A}]_{il}}, & |[\boldsymbol{A}]_{il}| \geq \frac{1}{2} \\ 0, & |[\boldsymbol{A}]_{il}| < \frac{1}{2} \end{cases}. \tag{5}$$

The fully-connected phase shifters and switches network is presented in Fig. 1a.

S2) **Fully Connected Phase Shifters Network:** (architecture A1 in [8]). In this case, each antenna is connected to an RF chain through an independent phase shifter, without a switch. Thus, $\boldsymbol{W}_{RF}$ is a unimodular matrix: $\mathcal{W}^{N_r \times N_{RF}^r} = \{\boldsymbol{W} \in \mathbb{C}^{N_r \times N_{RF}^r} : |w_{ij}| = 1\}$. Here we have

$$[\boldsymbol{P}_{\mathcal{W}}(\boldsymbol{A})]_{il} = e^{j2\pi\angle[\boldsymbol{A}]_{il}}. \tag{6}$$

Figure 1b. demonstrates this setting.

S3) **Switching Network:** (architecture A5 in [8]). This is an antenna selection scheme, where each RF chain is preceded by a single switch that can toggle between the N_r antennas. A total of N_{RF}^r antennas are selected and sampled. It follows that $\boldsymbol{W}_{RF}$ is a partial permutation matrix: $\mathcal{W}^{N_r \times N_{RF}^r} = \{\boldsymbol{W} \in \mathbb{C}^{N_r \times N_{RF}^r} : w_{ij} \in$
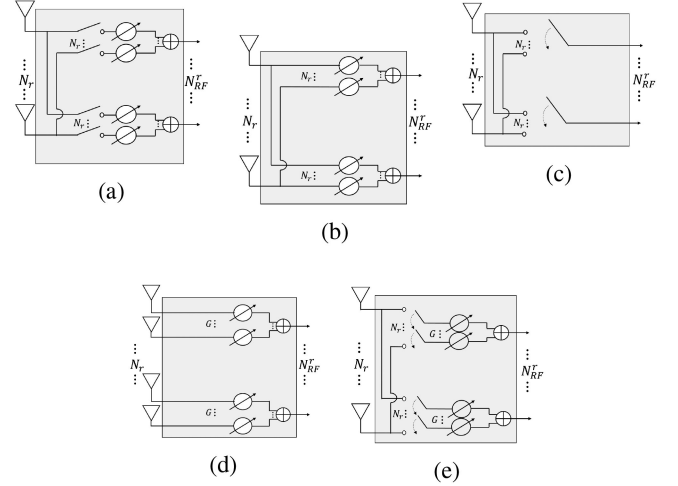

Fig. 1. Combiner hardware schemes. (1a) S1: Fully connected phase shifters and switches network, (1b) S2: Fully connected phase shifters network, (1c) S3: Switching network, (1d) S4: Fixed partially connected phase shifters network with sub-arrays, and (1e) S5: Flexible partially connected phase shifters network with sub-arrays.

$\{0, 1\}, \|\boldsymbol{w}_j\|_0 = 1\}$. The projection $\boldsymbol{P}_{\mathcal{W}}(\boldsymbol{A})$ chooses the entry with largest absolute value in each column of $\boldsymbol{A}$ and sets the corresponding entry of the output to 1, while all other entries are set to 0. This setting is shown in Fig. 1c. Another structure is the switching network with sub-arrays (architecture A6 in [8]), where the switching range is limited to a certain subset of antennas for each RF chain. Note that in switching networks, phase shifters are unnecessary, since each input can be processed independently at BB.

S4) **Partially Connected Phase Shifters Network with Fixed Sub Arrays:** (architecture A2 in [8]). This scheme divides the array into (possibly overlapping) sub-arrays of size G. Each sub-array operates as a fully-connected phase shifter network with a single RF chain. This results in the feasible set $\mathcal{W}^{N_r \times N_{RF}^r} = \{\boldsymbol{W} \in \mathbb{C}^{N_r \times N_{RF}^r} : |w_{ij}| = 1, \forall i \in \mathcal{S}_j, |w_{ij}| = 0, \forall i \notin \mathcal{S}_j\}$, with $\mathcal{S}_j$ the group of indices corresponding to antennas that belong to the jth sub-array. In this case $\boldsymbol{P}_{\mathcal{W}}(\boldsymbol{A})$ applies the mapping in (6) to the G entries of $\boldsymbol{a}_j$ that belong to $\mathcal{S}_j$, and sets all others to 0. The fixed sub-arrays network is presented in Fig. 1d. The parameter G represents the connectivity factor; for $G = N_r$, we get the fully-connected network S2.

S5) **Flexible Partially Connected Phase Shifters Network with Sub Arrays:** This architecture is similar to the previous one, except that the contributing antennas to each RF chain are not fixed, but can be optimized, i.e. the subgroups $\mathcal{S}_j$ are flexible. This is implemented using a N_r-to-1 switch that precedes the phase shifters. The corresponding feasible set is $\mathcal{W}^{N_r \times N_{RF}^r} = \{\boldsymbol{W} \in \mathbb{C}^{N_r \times N_{RF}^r} : |w_{ij}| \in \{0, 1\}, \|\boldsymbol{w}_j\|_0 = G\}$. The function $\boldsymbol{P}_{\mathcal{W}}(\boldsymbol{A})$ in this case chooses the G entries with largest absolute value in each column of $\boldsymbol{A}$ and applies (6) to them while setting all others to 0.

	S1	S2	S3	S4	S5
Phase Shifters #	$N_r \cdot N_{RF}^r$	$N_r \cdot N_{RF}^r$	0	$G \cdot N_{RF}^r$	$G \cdot N_{RF}^r$
Switches #	$N_r \cdot N_{RF}^r$	0	N_{RF}^r	0	$G \cdot N_{RF}^r$
Switch Type	on-off	-	N_r-to-1	-	N_r-to-1

The networks above constitute some of the main classes of existing analog architectures. They present different levels of challenge in terms of hardware complexity, as in Table I. For a complete power consumption comparison, the reader is referred to the example in [8]. One may define many additional architectures based on the above networks by modifying their components and connectivity factors.

III. MSE MINIMIZATION

To optimally design the precoder and combiner we consider the MSE minimization problem in (4).

Since there are no constraints on W_{BB} in (4), it can be chosen as any $N_{RF}^r \times N_{RF}^r$ matrix, including the linear MMSE estimator of s from the measurements $\tilde{y} = W_{RF}^* y$. This estimator depends on the matrices F_{RF}, F_{BB}, W_{RF} and is given by

$$W_{BB,opt}^* = \bar{H}^* W_{RF} \left[W_{RF}^* \left(\bar{H} \bar{H}^* + R_z \right) W_{RF} \right]^{-1}, \quad (7)$$

with

$$\bar{H} = \sqrt{p_r} H F_{RF} F_{BB}. \quad (8)$$

The resulting estimate is

$$\hat{s} = \bar{H}^* W_{RF} \left[W_{RF}^* \left(\bar{H} \bar{H}^* + R_z \right) W_{RF} \right]^{-1} W_{RF}^* y, \quad (9)$$

and its MSE is equal to

$$\mathbb{E}[\|s - \hat{s}\|^2] = N_s - \text{tr}(\bar{H}^* W_{RF} [W_{RF}* \left(\bar{H} \bar{H}^* + R_z \right)$$
$$W_{RF}]^{-1} W_{RF}^* \bar{H}). \quad (10)$$

The digital combiner of (7) is the optimal linear estimator in the MSE sense for any given precoders F_{RF}, F_{BB} and analog combiner W_{RF}. Thus, our remaining goal is to design W_{RF}, F_{RF}, F_{BB} to minimize (10). This is equivalent to the following maximization problem:

$$\max_{W_{RF}, F_{RF}, F_{BB}} f\left(W_{RF}, F_{RF}, F_{BB} \right)$$

$$\text{s.t.:} \quad F_{RF} \in \mathcal{F}^{N_t \times N_{RF}^t}, \ \|F_{RF} F_{BB}\|_F^2 \leq N_s,$$

$$W_{RF} \in \mathcal{W}^{N_r \times N_{RF}^r}, \quad (11)$$

with

$$f\left(W_{RF}, F_{RF}, F_{BB} \right) = \text{tr}\big(W_{RF}^* \bar{H} \bar{H}^* W_{RF}$$
$$\left[W_{RF}^* \left(\bar{H} \bar{H}^* + R_z \right) W_{RF} \right]^{-1} \big). \quad (12)$$

Similar to the case considered in [4], the joint optimization problem (11) is non-convex and has no known solution. Hence, as in previous works [4], [11], [13], we simplify the problem by

decoupling it. First, in Section IV, we optimize the precoders F_{RF}, F_{BB} given W_{RF}. Then, in Section V, we assume fixed F_{RF}, F_{BB} and optimize the combiner W_{RF}.

IV. PRECODER DESIGN

We now consider the problem of designing the precoder $F = F_{RF} F_{BB}$. To this end we assume a fixed analog combiner and rewrite (11) as

$$\max_{F_{RF}, F_{BB}} \ \text{tr} \left(\tilde{H} F F^* \tilde{H}^* \left[\tilde{H} F F^* \tilde{H}^* + \tilde{R} \right]^{-1} \right) \quad (13)$$

$$\text{s.t.:} \quad F_{RF} \in \mathcal{F}^{N_t \times N_{RF}^t}, \ \|F_{RF} F_{BB}\|_F^2 \leq N_s,$$

with $\tilde{H} = \sqrt{p_r} W_{RF}^* H$ and $\tilde{R} = W_{RF}^* R_z W_{RF}$. If we relax the constraint $F_{RF} \in \mathcal{F}^{N_t \times N_{RF}^t}$ to the fully-digital case $F_{RF} \in \mathbb{C}^{N_t \times N_{RF}^t}$, then (13) has a closed form solution [17]

$$F_{opt} = V \Phi T \quad (14)$$

where V contains the first N_{RF}^t eigenvectors of the matrix $\tilde{H}^* \tilde{R}^{-1} \tilde{H}$, Φ is an $N_{RF}^t \times N_{RF}^t$ diagonal matrix with power allocation weights as in [17], and T denotes any $N_{RF}^t \times N_{RF}^t$ unitary matrix. It follows that there is a set of optimal solutions, one for every unitary T.

Previous works [4], [6]–[8], [11], [13] considered $T = I_{N_{RF}^t}$ and suggested to approximate F_{opt} with a decomposition $F_{RF} F_{BB}$, which yields the problem

$$\min_{F_{RF}, F_{BB}} \ \|F_{opt} - F_{RF} F_{BB}\|_F^2$$

$$\text{s.t.:} \quad F_{RF} \in \mathcal{F}^{N_t \times N_{RF}^t}, \ \|F_{RF} F_{BB}\|_F^2 \leq N_s. \quad (15)$$

This approach is motivated by the approximation in [4] which shows that minimizing (15) approximately maximizes the system's spectral efficiency. However, these solutions suffer from several disadvantages due to dictionary constraints or high complexity. None of the above works take advantage of the flexibility in choosing T, which we show below can boost the performance of existing solutions with only a small computational price.

Specifically, we exploit the flexibility in the choice of T, and find the unitary matrix that results in the smallest approximation gap $\|V \Phi T - F_{RF} F_{BB}\|_F^2$. To this end, we develop an alternating minimization framework inspired by [18], that alternately optimizes over F_{RF}, F_{BB} and T. In the simulations in Section VI, we demonstrate that by adding the optimization over T, we are able to improve the performance of state-of-the-art algorithms, with no substantial increase in complexity.

A. Alt-MaG - Alternating Minimization of Approximation Gap

Plugging (14) into (15) and adding T as an optimization variable, our problem becomes

$$\min_{T, F_{RF}, F_{BB}} \|V\Phi T - F_{RF} F_{BB}\|_F^2$$

$$\text{s.t.:} \quad F_{RF} \in \mathcal{F}^{N_t \times N_{RF}^t}, \ \|F_{RF} F_{BB}\|_F^2 \le N_s, \quad (16)$$

$$T \in \mathcal{U}^{N_{RF}^t},$$

with $\mathcal{U}^M$ the set of all $M \times M$ unitary matrices. To approximate the solution of (16), we consider an alternating minimization approach. First, we fix F_{RF}, F_{BB} and solve

$$\min_{T} \quad \|V\Phi T - F_{RF} F_{BB}\|_F^2$$

$$\text{s.t.:} \quad T \in \mathcal{U}^{N_{RF}^t}. \quad (17)$$

Next, using the resulting T, we solve

$$\min_{F_{RF}, F_{BB}} \quad \|V\Phi T - F_{RF} F_{BB}\|_F^2$$

$$\text{s.t.:} \quad F_{RF} \in \mathcal{F}^{N_t \times N_{RF}^t}, \|F_{RF} F_{BB}\|_F^2 \le N_s, \quad (18)$$

and repeat iteratively.

If both (17) and (18) can be solved, then the objective value decreases in each step, and since it is bounded from below, the algorithm will converge to a local optimum. However, while (17) has a (closed form) optimal solution, problem (18) is a special case of (15), which has no known solution. To attain a sub optimal solution, any of the mentioned algorithms [4], [6]–[9], [11], [13] may be used (provided it is compatible with the hardware choice). Each of these solutions will result in a different algorithm from the Alt-MaG family.

A closed form solution to problem (17) is given in the next theorem.

Theorem 1: Given the singular value decomposition $F_{BB}^* F_{RF}^* V\Phi = \tilde{U}\Lambda\tilde{V}^*$, the optimal solution T_{opt} to (17) is given by

$$T_{opt} = \tilde{V}\tilde{U}^*. \quad (19)$$

Proof: First, note that $\|V\Phi T - F_{RF} F_{BB}\|_F^2 = \|V\Phi\|_F^2 + \|F_{RF} F_{BB}\|_F^2 - 2\Re(\text{tr}(F_{BB}^* F_{RF}^* V\Phi T))$. Thus, it is sufficient to maximize $\Re(\text{tr}(F_{BB}^* F_{RF}^* V\Phi T))$. Denote $\Lambda = \Omega^2$. Then,

$$\Re(\text{tr}(F_{BB}^* F_{RF}^* V\Phi T)) \le |\text{tr}(F_{BB}^* F_{RF}^* V\Phi T)|$$

$$= \left|\text{tr}((\tilde{U}\Omega)(T^*\tilde{V}\Omega)^*)\right|$$

$$\underset{(*)}{\le} \sqrt{\text{tr}(\tilde{U}\Omega^2\tilde{U}^*)\text{tr}(T^*\tilde{V}\Omega^2\tilde{V}^* T)}$$

$$= \text{tr}(\Omega^2),$$

where $(*)$ stems from the Cauchy-Schwarz inequality. For $T = \tilde{V}\tilde{U}^*$, the upper bound is achieved with equality. ∎

The resulting family of Alt-MaG algorithms is outlined in Algorithm 1. The stopping criteria in Algorithm 1 is a threshold on the approximation gap. Another option for this criteria is a threshold on the difference of approximation gaps between

---

Algorithm 1: Alt-MaG - Alternating Minimization of Approximation Gap.

Input: fully-digital precoder $V\Phi$, threshold t
Output: digital precoder F_{BB}, analog precoder F_{RF}
Initialize $T = I_{N_{RF}^t}, F_{RF} = 0, F_{BB} = 0$
While $\|V\Phi T - F_{RF} F_{BB}\|_F^2 \ge t$ do:
  1) **Calculate** (F_{RF}, F_{BB}) from (18)
  2) **Calculate** the singular value decomposition
    $F_{BB}^* F_{RF}^* V\Phi = \tilde{U}\Lambda\tilde{V}^*$
  3) **Set** $T = \tilde{V}\tilde{U}^*$

---

the former and current iterations, i.e. $\Delta^{(i)} = \|V\Phi T^{(i-1)} - F_{RF}^{(i-1)} F_{BB}^{(i-1)}\|_F^2 - \|V\Phi T^{(i)} - F_{RF}^{(i)} F_{BB}^{(i)}\|_F^2$.

The convergence of Alt-MaG depends on the specific algorithm used for the hybrid decomposition step. If the method used obtains an optimal solution to (18), then the objective function $\|V\Phi T - F_{RF} F_{BB}\|_F^2$ does not increase in each iteration and since it is non-negative Alt-MaG will converge. If the hybrid decomposition algorithm is sub-optimal, then it is possible that the decomposition step will result in an increase in the approximation gap. In practice, this issue can be addressed by checking that the approximation gap did not increase after each decomposition step. In Section VI we demonstrate that Alt-MaG typically converges after very few iterations.

Next we suggest a possible simplification to (18) that can be used with any of the schemes S1-S5, and results in a simple closed form solution for F_{RF}, F_{BB}.

B. MaGiQ - Minimal Gap Iterative Quantization

The complexity of Algorithm 1 is determined by the method used in step 1 and could be accordingly high. One approach that yields a low complexity algorithm, is approximating $V\Phi T$ by an analog precoder only, setting the digital precoder to $F_{BB} = I_{N_{RF}^t}$. That is, in every iteration, solving

$$\min_{F_{RF}} \quad \|V\Phi T - F_{RF}\|_F^2$$

$$\text{s.t.:} \quad F_{RF} \in \mathcal{F}^{N_t \times N_{RF}^t}. \quad (20)$$

The benefit of this approach is the existence of a simple, optimal, closed form solution to (20), given by

$$F_{RF} = P_{\mathcal{F}}(V\Phi T), \quad (21)$$

with $P_{\mathcal{F}}(\cdot)$ defined in Section II.

Once F_{RF} and T converge, F_{BB} is calculated as the solution to

$$\min_{F_{BB}} \quad \|V\Phi T - F_{RF} F_{BB}\|_F^2$$

$$\text{s.t.:} \quad \|F_{RF} F_{BB}\|_F^2 \le N_S. \quad (22)$$

Note that F_{RF} depends on $V\Phi T$ which is a function of the random channel and interference. With high probability, it has full column rank. In this case, (22) has a closed form solution

$$F_{BB} = [F_{RF}^* F_{RF}]^{-1} F_{RF}^* V\Phi T. \quad (23)$$

Algorithm 2: MaGiQ - Minimal Gap Iterative Quantization.

Input: fully-digital precoder $\boldsymbol{V\Phi}$, threshold t
Output: digital precoder $\boldsymbol{F}_{BB}$, analog precoder $\boldsymbol{F}_{RF}$
Initialize $\boldsymbol{T} = \boldsymbol{I}_{N_{RF}^t}$, $\boldsymbol{F}_{RF} = \boldsymbol{0}$, $\boldsymbol{F}_{BB} = \boldsymbol{I}_{N_{RF}^t}$
While $\|\boldsymbol{V\Phi T} - \boldsymbol{F}_{RF}\|_F^2 \geq t$ do:
 1) **Calculate** $\boldsymbol{F}_{RF} = \boldsymbol{P}_{\mathcal{F}}(\boldsymbol{V\Phi T})$
 2) **Calculate** the singular value decomposition
    $\boldsymbol{F}_{RF}^* \boldsymbol{V\Phi} = \tilde{\boldsymbol{U}}\boldsymbol{\Lambda}\tilde{\boldsymbol{V}}^*$
 3) **Set** $\boldsymbol{T} = \tilde{\boldsymbol{V}}\tilde{\boldsymbol{U}}^*$
Calculate $\boldsymbol{F}_{BB} = [\boldsymbol{F}_{RF}^* \boldsymbol{F}_{RF}]^{-1} \boldsymbol{F}_{RF}^* \boldsymbol{V\Phi T}$

Since the optimal solution $\boldsymbol{V\Phi T}$ obeys the transmit power constraint $\|\boldsymbol{V\Phi T}\|_F^2 \leq N_S$, it follows that

$$\|\boldsymbol{F}_{RF}\boldsymbol{F}_{BB}\|_F^2 = \|\boldsymbol{F}_{RF}[\boldsymbol{F}_{RF}^*\boldsymbol{F}_{RF}]^{-1}\boldsymbol{F}_{RF}^*\boldsymbol{V\Phi T}\|_F^2$$
$$= \|\boldsymbol{P}_{\boldsymbol{F}_{RF}}\boldsymbol{V\Phi T}\|_F^2 \leq \|\boldsymbol{V\Phi T}\|_F^2 \leq N_S.$$

Therefore, (23) complies with the transmit power constraint.

MaGiQ is summarized in Algorithm 2. Since the non-negative objective function $\|\boldsymbol{V\Phi T} - \boldsymbol{F}_{RF}\|_F^2$ does not increase at each iteration of Algorithm 2, the algorithm converges. In the simulations in Section VI, we demonstrate that MaGiQ has lower MSE than other low-complexity methods in the case of very few RF chains.

The dominant operation in each iteration of MAGiQ is the singular value decomposition of the $N_t \times N_{RF}^t$ matrix $\boldsymbol{F}_{RF}^* \boldsymbol{V\Phi}$, which has time complexity of order $O(N_t(N_{RF}^t)^2)$. The other two steps are matrix multiplication of $N_t \times N_{RF}^t$ and $N_{RF}^t \times N_{RF}^t$ matrices, and the projection operation $\boldsymbol{P}_{\mathcal{F}}(\boldsymbol{V\Phi T})$, which consists of a mix of maximum operations and per entry multiplications. Therefore, those are negligible compared to the decomposition step. The total complexity of MaGiQ depends on the choice of stopping criteria, which determines the number of iterations. A good choice results in a number of iterations that is linear in N_{RF}^t. In this case, the complexity of the algorithm is $O(N_t(N_{RF}^t)^3)$.

A version of Algorithm 2, PE-AltMin, has been previously suggested in [11] for the scheme S2, as an optimization of an upper bound on (18). There, the authors assumed that the optimal $\boldsymbol{F}_{BB}$ is an orthogonal matrix of the form $\boldsymbol{F}_{BB} = \alpha \boldsymbol{T}$, and considered the problem

$$\min_{\boldsymbol{T}, \alpha, \boldsymbol{F}_{RF}} \|\boldsymbol{V\Phi} - \alpha \boldsymbol{F}_{RF}\boldsymbol{T}\|_F^2$$

$$\text{s.t.}: \quad \boldsymbol{F}_{RF} \in \mathcal{F}^{N_t \times N_{RF}^t}, \; \|\alpha \boldsymbol{F}_{RF}\boldsymbol{T}\|_F^2 = N_s, \quad (24)$$

$$\boldsymbol{T} \in \mathcal{U}^{N_{RF}^t}.$$

Setting $\alpha = \frac{\sqrt{N_S}}{\|\boldsymbol{F}_{RF}\boldsymbol{T}\|_F}$, and using some mathematical manipulations, they bounded the objective in (24) from above with the expression $\|\boldsymbol{V\Phi T}^* - \boldsymbol{F}_{RF}\|_F^2$. After optimizing the upper bound over $\boldsymbol{T}$ and $\boldsymbol{F}_{RF}$ alternately, they set $\boldsymbol{F}_{BB}$ as $\boldsymbol{F}_{BB} = \frac{\sqrt{N_S}}{\|\boldsymbol{F}_{RF}\boldsymbol{T}\|_F}\boldsymbol{T}$. In contrast, we do not limit $\boldsymbol{F}_{BB}$ to be orthogonal. After optimizing $\boldsymbol{T}$ and $\boldsymbol{F}_{RF}$ alternately, we calculate $\boldsymbol{F}_{BB}$ as in (23), thus exploiting an additional flexibility in its structure. In the simulations in Section VI we

compare both methods and demonstrate that MaGiQ enjoys better performance. The main difference between this approach and MaGiQ, is that while we exploit the degree of freedom in the fully-digital precoder, PE-AltMin restricts the set of possible digital precoders to orthogonal matrices alone, which degrades performance.

Alt-MaG and MaGiQ where developed for MSE minimization, but can be generalized to other performance criteria, by replacing the optimal unconstrained solution expressions. For example, when considering the system's spectral efficiency as in [4], [11], the optimal solution is (14) with $\boldsymbol{\Phi}$ now being a diagonal matrix with the power allocation weights given by water filling [17].

C. Optimality of MaGiQ

One advantage of MaGiQ over other existing techniques is that in some special cases it converges to the optimal fully-digital solution, as we show in the following proposition.

Proposition 1: Define $\boldsymbol{F}_{opt}$ as in (14), and assume that $\boldsymbol{\Phi}$ has positive values on its diagonal. Denote $\tilde{\boldsymbol{F}}$ the hybrid precoder produced by MAGiQ for the input $\boldsymbol{F}_{opt}$. If $\boldsymbol{V\Psi} \in \mathcal{F}^{N_t \times N_{RF}^t}$, for some diagonal, positive definite matrix $\boldsymbol{\Psi}$, then

$$\tilde{\boldsymbol{F}} = \boldsymbol{V\Phi}.$$

Proposition 1 implies that if each column of $\boldsymbol{V}$ lies in the feasible set $\mathcal{F}^{N_t \times 1}$ up to some scaling, then MaGiQ will produce a globally optimal solution. This property is not assured in other algorithms, as demonstrated in the simulations in Section VI.

Proof: For simplicity, we consider here the fully-connected phase shifter network S2. However, Proposition 1 holds for any hardware scheme with the same condition $\boldsymbol{V\Psi} \in \mathcal{F}^{N_t \times N_{RF}^t}$, and similar proofs can be constructed accordingly.

For S2, $\boldsymbol{V\Psi} \in \mathcal{F}^{N_t \times N_{RF}^t}$ implies that $\boldsymbol{V}$ has columns with constant modulus. In the first iteration of MaGiQ, $\boldsymbol{T}$ is initialized as $\boldsymbol{T} = \boldsymbol{I}_{N_{RF}^t}$. Since $\boldsymbol{\Phi}$ is a diagonal matrix with positive diagonal values, step 1 of the algorithm leads to

$$\boldsymbol{F}_{RF} = \boldsymbol{P}_{\mathcal{F}}(\boldsymbol{V\Phi}) = \boldsymbol{V\Psi}.$$

It follows that $\boldsymbol{F}_{RF}^* \boldsymbol{V\Phi} = \boldsymbol{\Psi\Phi}$, which is diagonal. Thus, step 3 yields

$$\boldsymbol{T} = \boldsymbol{I}_{N_{RF}^t}$$

and the algorithm converges after a single iteration. For $\boldsymbol{F}_{BB}$ we get

$$\boldsymbol{F}_{BB} = [\boldsymbol{F}_{RF}^*\boldsymbol{F}_{RF}]^{-1}\boldsymbol{F}_{RF}^*\boldsymbol{V\Phi} = \boldsymbol{\Psi}^{-1}\boldsymbol{\Phi},$$

and the received hybrid precoder is $\tilde{\boldsymbol{F}} = \boldsymbol{V\Phi}$. ∎

Note that the diagonal matrix $\boldsymbol{\Phi}$ represents non-negative weights [17]. If one of the weights is equal to zero, then the corresponding column in the optimal fully-digital precoder is all zeros. In that case, we can drop the relevant column, and use the above proposition with the remaining fully-digital precoder.

One example of a scenario in which the conditions of Proposition 1 hold, is a fully-connected phase shifter precoder (for simplicity we assume a fully-digital combiner) with $\boldsymbol{R}_z = \sigma_z^2 \boldsymbol{I}_{N_r}$,

and circulant channel matrix, that is

$$\boldsymbol{H} = \boldsymbol{A}_r \boldsymbol{\Lambda} \boldsymbol{A}_t^*, \tag{25}$$

where $\boldsymbol{A}_r$, $\boldsymbol{A}_t$ are DFT matrices and $\boldsymbol{\Lambda}$ is a diagonal gain matrix. In this case, the singular vectors of $\boldsymbol{H}^* \boldsymbol{R}_z^{-1} \boldsymbol{H}$ are columns of the DFT matrix which are unimodular, and thus lie in $\mathcal{F}^{N_t \times 1}$ for S2. Therefore, from Proposition 1, MaGiQ produces the optimal solution (14).

A common special case of (25), is the well-known narrowband mmWave clustered channel [19]–[21], with a single ray at each cluster and asymptotic number of antennas. This model consists of N_{cl} clusters with N_{ray} propagating rays, each ray associated with transmit and receive directions, and complex gain. The channel matrix can be written as

$$\boldsymbol{H} = \sqrt{\frac{N_t N_r}{N_{cl} N_{ray}}} \sum_{i=1}^{N_{cl}} \sum_{l=1}^{N_{ray}} \alpha_{il} \boldsymbol{a}_r \left(\phi_{il}^r, \theta_{il}^r \right) \boldsymbol{a}_t \left(\phi_{il}^t, \theta_{il}^t \right)^*, \tag{26}$$

with α_{il} the complex gain of the lth ray in the ith cluster, and $(\phi_{il}^t, \theta_{il}^t), (\phi_{il}^r, \theta_{il}^r)$ the azimuth and elevation angles of departure and arrival for the lth ray in the ith cluster respectively. The vectors $\boldsymbol{a}_t(\phi_{il}^t, \theta_{il}^t)$ and $\boldsymbol{a}_r(\phi_{il}^r \theta_{il}^r)$ represent the transmit and receive array responses, and depend on the array geometry.

For $N_{ray} = 1$, (26) can be written as (25) with $\boldsymbol{\Lambda}$ a $N_{cl} \times N_{cl}$ diagonal matrix with the elements $\sqrt{\frac{N_t N_r}{N_{cl} N_{ray}}} \alpha_{il}$ on its diagonal, and $\boldsymbol{A}_r$, $\boldsymbol{A}_t$ being steering matrices composed of the vectors $\boldsymbol{a}_r(\phi_{il}^r, \theta_{il}^r)$ and $\boldsymbol{a}_t(\phi_{il}^t, \theta_{il}^t)$ respectively. As N_r, N_t grow to infinity, the matrices $\boldsymbol{A}_r$, $\boldsymbol{A}_t$ become orthogonal. Hence, in a noise-limited system, $\boldsymbol{V}$ is asymptotically equal to the steering vectors (up to some normalization constant) and thus unimodular.

The above example can be generalized easily to a hybrid fully-connected phase shifter combiner rather than a fully-digital one.

To summarize the results of this section, we presented two new algorithms that benefit from optimizing over the unitary matrix $\boldsymbol{T}$; the low complexity MaGiQ that uses a simple orthogonal projection step to comply with the feasible constraint, and the more general Alt-Mag which can be used with other methods to solve problem (18) in its first step. The choice of algorithm should be made according to the complexity requirement. For example, if the computational load is not a limiting factor, then Alt-MaG along with MO-AltMin from [11] is a good choice. In Section VI we demonstrate that MaGiQ yields low MSE with very few RF chains, and that the additional optimization over the unitary matrix in Alt-MaG improves the performance without a substantial increase in runtime.

V. ANALOG COMBINER DESIGN

We now approach the design of analog combiner

$$\boldsymbol{W} = \boldsymbol{W}_{BB} \boldsymbol{W}_{RF}. \tag{27}$$

For this purpose we assume a fixed precoder, that is, $\bar{\boldsymbol{H}}$ in (8) is fixed and known.

In (7), we derived the optimal $N_{RF}^r \times N_{RF}^r$ digital combiner, given the hybrid decomposition (27), and reduced the problem to $\boldsymbol{W}_{RF}$ alone. A different approach is to first allow the entire $N_r \times N_{RF}^r$ hybrid combiner to be digital, and then try and approximate the fully-digital solution with a hybrid decomposition, similar to the precoder optimization in the previous section.

This approach was adopted in [4], [9]. There, the authors begun by allowing $\boldsymbol{W}$ to be fully-digital, that is $\boldsymbol{W} \in \mathbb{C}^{N_r \times N_{RF}^r}$, and solved problem (4) for fixed precoders. This yields the MMSE estimator of $\boldsymbol{s}$ from $\boldsymbol{y}$, given by

$$\boldsymbol{W}_{mmse} = \boldsymbol{B}^{-1} \bar{\boldsymbol{H}}, \tag{28}$$

with

$$\boldsymbol{B} = \bar{\boldsymbol{H}} \bar{\boldsymbol{H}}^* + \boldsymbol{R}_z. \tag{29}$$

It was shown in [4] that minimizing (4) (for fixed precoders) is equivalent to solving the following optimization problem:

$$\min_{\boldsymbol{W}_{RF}, \boldsymbol{W}_{BB}} \| \boldsymbol{B}^{\frac{1}{2}} \left(\boldsymbol{W}_{mmse} - \boldsymbol{W}_{RF} \boldsymbol{W}_{BB} \right) \|_F^2$$

$$\text{s.t.:} \quad \boldsymbol{W}_{RF} \in \mathcal{W}^{N_r \times N_{RF}^r}. \tag{30}$$

That is, finding the hybrid decomposition of $\boldsymbol{W}_{mmse}$ that minimizes the weighted norm in (30).

Unlike the precoder case, here (30) and (4) are equivalent. Motivated by this, the authors in [4], [9] assumed a multipath channel structure as in (26), which implies that the optimal combiner is a sparse sum of steering vectors. They then suggested a variation of simultaneous OMP (SOMP) to solve (30), that chooses the analog combiner vectors from a steering dictionary and sets the digital combiner as the corresponding weights. However, this algorithm suffers from degraded performance due to the dictionary constraint.

By dropping the weights matrix $\boldsymbol{B}^{\frac{1}{2}}$, (30) becomes

$$\min_{\boldsymbol{W}_{RF}, \boldsymbol{W}_{BB}} \| \boldsymbol{W}_{mmse} - \boldsymbol{W}_{RF} \boldsymbol{W}_{BB} \|_F^2$$

$$\text{s.t.:} \quad \boldsymbol{W}_{RF} \in \mathcal{W}^{N_t \times N_{RF}^t}, \tag{31}$$

which constitutes an upper bound on (30) (divided by the constant factor $\| \boldsymbol{B}^{\frac{1}{2}} \|_F^2$), and is identical (up to the power constraint) to the precoder problem (15) in the previous section. Hence the methods in [6]–[8], [11], [13] can be used to solve it. However, solving (31) is only optimizing an upper bound on the original objective, and is thus sub-optimal.

A. MaGiQ for Combiner Design

As opposed to previous works, we impose the hybrid decomposition (27), and optimize (4) over both $\boldsymbol{W}_{BB}$ and $\boldsymbol{W}_{RF}$, as in Section III. This leads to the problem of minimizing (10) over $\boldsymbol{W}_{RF}$, which is equivalent to

$$\max_{\boldsymbol{W}_{RF}} \text{tr} \left(\boldsymbol{W}_{RF}^* \boldsymbol{A} \boldsymbol{W}_{RF} \left[\boldsymbol{W}_{RF}^* \boldsymbol{B} \boldsymbol{W}_{RF} \right]^{-1} \right)$$

$$\text{s.t.:} \quad \boldsymbol{W}_{RF} \in \mathcal{W}^{N_r \times N_{RF}^r}, \tag{32}$$

with $\boldsymbol{A} = \bar{\boldsymbol{H}} \bar{\boldsymbol{H}}^*$, $\boldsymbol{B}$ as in (29), and $\mathcal{W}$ the feasible set of the given hardware scheme described in Section II. Note that since $\boldsymbol{R}_z$ is positive definite, it follows that $\boldsymbol{B}$ is invertible. In contrast to the previous section, the problem in (32) is a function of the

analog combiner alone, and does not depend on the dimensions of the digital combiner. Therefore, algorithms developed to solve (32) are the same for both $N_s = N_{RF}^r$ and $N_s < N_{RF}^r$. The only difference between these two cases is the dimension of the digital combiner in (7).

Proposition 2: The optimal fully-digital solution to (32), is given by

$$W_{opt} = B^{-\frac{1}{2}} U S, \qquad (33)$$

where U contains the first N_{RF}^r eigenvectors of the matrix $B^{-\frac{1}{2}} A B^{-\frac{1}{2}}$, with $A = \bar{H}\bar{H}^*$, and $\bar{H}, B$ are as in (8), and (29). The matrix S is any $N_{RF}^r \times N_{RF}^r$ invertible matrix.

Proof: The fully-digital problem corresponding to (32) is

$$\max_{W_{RF}} \quad \text{tr}\left(W_{RF}^* A W_{RF} \left[W_{RF}^* B W_{RF}\right]^{-1}\right). \qquad (34)$$

Let $Q \in \mathbb{C}^{N_r \times N_{RF}^r}$ be defined by $Q = B^{\frac{1}{2}} W_{RF}$. Then the objective in (34) equals to $\text{tr}(P_Q B^{-\frac{1}{2}} A B^{-\frac{1}{2}})$. Let V be a $N_r \times N_{RF}^r$ matrix with orthogonal columns that span $\mathcal{R}(Q)$. Then, $P_Q = V V^*$ and $Q = V S$ for some invertible $N_{RF}^r \times N_{RF}^r$ matrix S. Thus, the objective becomes $\text{tr}(V^* B^{-\frac{1}{2}} A B^{-\frac{1}{2}} V)$ which is maximized by choosing V as the first N_{RF}^r eigenvectors of $B^{-\frac{1}{2}} A B^{-\frac{1}{2}}$, i.e. $V = U$. Therefore,

$$Q = U S,$$

which yields the solution (33). ∎

Similarly to the previous section, we now approximate the optimal unconstrained solution (33) with an analog combiner, while seeking an S that yields a minimal approximation gap between the two.

In (33), S is only required to be invertible, in contrast to the unitary constraint in (14). Hence, limiting it to $\mathcal{U}^{N_{RF}^r}$ is restrictive. However, this is a convenient way to enforce the invertibility constraint. The optimization problem we consider is therefore

$$\min_{W_{RF}, S} \|B^{-\frac{1}{2}} U S - W_{RF}\|_F^2$$

$$\text{s.t.} : \quad W_{RF} \in \mathcal{W}^{N_r \times N_{RF}^r}, \qquad (35)$$

$$S \in \mathcal{U}^{N_{RF}^r},$$

which can be solved using the MaGiQ approach presented in Section IV. Note that here Alt-MaG and MaGiQ coincide, since in step 1 of Alt-MaG the optimization is over W_{RF} alone. Once the algorithm converges, W_{BB} is calculated as in (7).

MaGiQ enjoys good performance with very few RF chains, but when the number of chains increases, other methods are preferable. One of the main factors that degrade MaGiQ, is that it only optimizes a bound (31) on (30), rather than directly maximizing (30) (which is equivalent to (32)). Next, we exploit the special structure of the ratio-trace objective in (32), and construct a greedy method for its direct maximization over W_{RF}. The proposed GRTM algorithm solves a ratio-of-scalars problem at each step and achieves low MSE when the number of RF chains increases.

Both GRTM and MaGiQ enjoy low complexity and each has its merits. For a small number of RF chains or a noise-limited

case with a fully connected phase shifters network and channel that has unimodular singular vectors, one should choose MaGiQ. For a more general channel model and increasing number of RF chains, GRTM is preferable.

B. GRTM - Greedy Ratio Trace Maximization

We now describe the GRTM approach for directly solving (32). The concept of GRTM is to solve (32) in a greedy manner, where in each iteration we add one RF chain and choose the optimal combiner vector to add to the previously K selected vectors, $1 \leq K \leq N_{RF}^r$.

Assume we have a solution $W_{RF}^{(K)} \in \mathcal{W}^{N_r \times K}$ for the K-sized problem, i.e. (32) with $N_{RF}^r = K$. We now want to add an additional RF chain, and compute the optimal column w such that $W_{RF}^{(K+1)} = [W_{RF}^{(K)} \ w]$. First, note that in order for $W_{RF}^{(K+1) *} B W_{RF}^{(K+1)}$ to be invertible and the objective in (32) to be well defined for the $(K+1)$-sized case, we require $w \notin \mathcal{R}(W_{RF}^{(K)})$. In practice, this condition implies that each RF chain contributes new and independent information with respect to the other chains. Given this condition, the $(K+1)$-sized optimization problem is

$$\max_{w} \quad \text{tr}\left(W_{RF}^{(K+1) *} A W_{RF}^{(K+1)} \left[W_{RF}^{(K+1) *} B W_{RF}^{(K+1)}\right]^{-1}\right)$$

$$\text{s.t.} : \quad w \in \mathcal{W}^{N_r \times 1}, \ w \notin \mathcal{R}\left(W_{RF}^{(K)}\right). \qquad (36)$$

In the next proposition, we show that (36) is equivalent to solving the following vector optimization problem, referred to as the base case:

$$\max_{w} \quad \frac{w^* C w}{w^* D w}$$

$$\text{s.t.} : \quad w \in \mathcal{W}^{N_r \times 1}, \ w^* D w > 0, \qquad (37)$$

where D and C are specific $N_r \times N_r$ positive semi definite (psd) matrices.

Using Proposition 3 leads to the GRTM solution of (32), where in each iteration we choose the best column vector to add to the previously selected combiner vectors by solving (37). The GRTM algorithm is summarized in Algorithm 3.

Proposition 3: Problems (37) and (36) are equivalent with

$$D = B^{\frac{1}{2}}\left(I_{N_r} - P_{B^{\frac{1}{2}} W_{RF}^{(K)}}\right) B^{\frac{1}{2}},$$

$$\gamma = \text{tr}\left(P_{B^{\frac{1}{2}} W_{RF}^{(K)}} B^{-\frac{1}{2}} A^{\frac{1}{2}} B^{-\frac{1}{2}}\right),$$

$$G = B^{\frac{1}{2}} P_{B^{\frac{1}{2}} W_{RF}^{(K)}} B^{-\frac{1}{2}} A^{\frac{1}{2}} - A^{\frac{1}{2}},$$

$$C = \gamma D + G G^*.$$

Proof: To prove the proposition, we rely on the following lemma:

Lemma 1: Let $\tilde{W} = [W \ w]$ and denote $Q = (W^* W)^{-1}$. Then [22, Ch. 3]

$$\left(\tilde{W}^* \tilde{W}\right)^{-1} = \begin{bmatrix} Q + \alpha Q W^* w w^* W Q^* & -\alpha Q W^* w \\ -\alpha w^* W Q^* & \alpha \end{bmatrix},$$

with $\alpha = \frac{1}{w^* w - w^* W Q W^* w}$.

Using Lemma 1 and straightforward algebraic operations we get equality between the two objectives. The first constraint is identical in both problems. It remains to show that the second constraints of (37) and (36) are equivalent.

Since B is invertible, $w \in \mathcal{R}(W_{RF}^{(K)})$ if and only if $B^{\frac{1}{2}} w \in \mathcal{R}(B^{\frac{1}{2}} W_{RF}^{(K)})$. Therefore, if $w \in \mathcal{R}(W_{RF}^{(K)})$, then

$$w^* D w = w^* B w - w^* B^{\frac{1}{2}} P_{B^{\frac{1}{2}} W_{RF}^{(K)}} B^{\frac{1}{2}} w$$

$$= w^* B w - w^* B^{\frac{1}{2}} B^{\frac{1}{2}} w = 0.$$

In the other direction, note that D is a non-negative Hermitian matrix, and can be decomposed as $D = Q Q^*$ for some Q. Thus, $w^* D w = 0$ if and only if $Q^* w = 0$. Multiplying both sides of the equation by Q yields $D w = B^{\frac{1}{2}} (I_{N_r} - P_{B^{\frac{1}{2}} W_{RF}^{(K)}}) B^{\frac{1}{2}} w = 0$. Since B is invertible, it follows that $(I_{N_r} - P_{B^{\frac{1}{2}} W_{RF}^{(K)}}) B^{\frac{1}{2}} w = 0$, or $B^{\frac{1}{2}} w \in \mathcal{R}(B^{\frac{1}{2}} W_{RF}^{(K)})$, which is equivalent to $w \in \mathcal{R}(W_{RF}^{(K)})$. Hence, we proved that

$$w \in \mathcal{R}\left(W_{RF}^{(K)}\right) \iff w^* D w = 0.$$

Since D is non-negative definite, $w^* D w \geq 0$, for all w. The previous connection then yields

$$w \notin \mathcal{R}\left(W_{RF}^{(K)}\right) \iff w^* D w > 0.$$

As there is equality between the objectives and feasible sets of (37) and (36), both problems are equivalent. ∎

Problem (37) has several advantages over (36): 1) its objective is a scalar ratio and does not involve matrix inversion. 2) This problem is both a constrained ratio-trace, trace-ratio [23] and a Rayleigh quotient problem, and therefore may be solved using techniques for either of these well known problems. These methods require adaptation to fit the additional hardware constraints, which is an interesting direction for future work.

One simple method for obtaining a (sub-optimal) solution to (37) is searching over a dictionary $\bar{W}$ with columns in $\mathcal{W}^{N_r \times 1}$, and calculating the objective value in (37) for each vector. The vector that corresponds to the largest objective is then chosen. This solution has low computational load thanks to the simplicity of the scalar ratio objective. The choice of dictionary depends on the channel model and hardware constraints. For a fully-connected scheme and a sparse mmWave channel as in (26), a steering vector dictionary used in [4] exploits the channel structure and yields good performance. For a more general model, Gaussian randomization can be used to construct a good dictionary. In this case, $\bar{W} = P_{\mathcal{W}}(X)$, with $P_{\mathcal{W}}(\cdot)$ defined in Section II, and where X is a random dictionary, commonly chosen as a matrix with columns drawn from $\mathcal{CN}(0, W_{opt} W_{opt}^*)$, with W_{opt} from (33). In the simulations section, we used the dictionary based solution with Gaussian randomization. To comply with the problem's second constraint, it is necessary to remove the selected column from the dictionary at each iteration. The other columns are, with high probability, not in $\mathcal{R}(W_{RF}^{(K)})$ due to the random complex-Gaussian distribution.

Simulations demonstrate that GRTM has lower MSE than MaGiQ when the number of RF chains increases. In that case,

---

Algorithm 3: GRTM.

Input effective channel $\bar{H}$, interference correlation R_z
Output analog combiner W_{RF}
Initialize $A = \bar{H} \bar{H}^*$, $B = \bar{H} \bar{H}^* + R_z$,
$C = A, D = B, W_{RF}^{(0)} = []$
For $K = 0 : N_{RF}^r - 1$:
  1) **Solve** the base case (37) to obtain w
  2) **Update** $W_{RF}^{(K+1)} = [W_{RF}^{(K)} \ w]$
  3) **Update**

$$D = B^{\frac{1}{2}} \left(I_{N_r} - P_{B^{\frac{1}{2}} W_{RF}^{(K+1)}} \right) B^{\frac{1}{2}}$$

$$\gamma = \text{tr}\left(P_{B^{\frac{1}{2}} W_{RF}^{(K+1)}} B^{-\frac{1}{2}} A^{\frac{1}{2}} B^{-\frac{1}{2}} \right)$$

$$G = B^{\frac{1}{2}} P_{B^{\frac{1}{2}} W_{RF}^{(K+1)}} B^{-\frac{1}{2}} A^{\frac{1}{2}} - A^{\frac{1}{2}}$$

$$C = \gamma D + G G^*$$

---

it outperforms other low complexity methods in various SNR, channel models, and hardware scenarios.

The algorithms in the precoder design section were derived for a fixed combiner, and vice versa. In practice, at least one of the beamformers is designed without the knowledge of the other. There are several approaches to address this issue. One possible choice is to first design the precoder assuming full receiver, i.e. no hybrid combiner, $W = I_{N_r}$, and then design the combiner given the resulting precoder, e.g. [4], [9]. Another option is to design the combiner assuming a full transmitter, i.e. $F = I_{N_t}$, e.g. [11], [13]. A third possibility is to design each beamformer assuming the other end uses the fully-digital optimal beamformer, e.g. [5]. In the simulations in Section VI we adopt the second approach, due to its simplicity.

C. Combiner Design for Kronecker Model Channel Estimation

Problem (32) arises in other communication problems, so that GRTM can be used to address those problems as well. One such scenario is MIMO channel estimation under a Kronecker model in the interference limited case [24], [25].

This problem consists of a single base station (BS) with N_{BS} antennas and $N_{RF} < N_{BS}$ RF chains, and K single-antenna users in a time-synchronized time division duplex (TDD) system. In the uplink channel estimation phase, each user sends τ training symbols to the BS, during which the channel is assumed to be constant.

The (discrete time) received signal at the BS can be written as

$$X = W_{RF}^* H S^T + Z, \qquad (38)$$

where $H \in \mathbb{C}^{N_{BS} \times K}$ is the desired channel between the users to the BS, $S \in \mathbb{C}^{\tau \times K}$ is the pilot sequence matrix, $W_{RF} \in \mathcal{W}^{N_{BS} \times N_{RF}}$ is the analog combiner and Z is the interference.

Both the channel and interference follow the *doubly correlated Kronecker model* [26]

$$H = R_r^{\frac{1}{2}} \bar{H} R_t^{\frac{1}{2}}, \quad Z = R_r^{\frac{1}{2}} \bar{Z} Q^{\frac{1}{2}}, \qquad (39)$$

with $\boldsymbol{R}_r \in \mathbb{C}^{N_{bs} \times N_{bs}}$ the BS's receive side correlation matrix, $\boldsymbol{R}_t \in \mathbb{C}^{K \times K}$ the transmit side correlation matrix of the users and $\boldsymbol{Q} \in \mathbb{C}^{K\tau \times \tau}$ the transmit side correlation matrix of the interference. The matrices $\bar{\boldsymbol{H}}^{N_{bs} \times K}, \bar{\boldsymbol{Z}} \in \mathbb{C}^{N_{bs} \times \tau}$ have independent entries with i.i.d complex-normal distribution. All correlation matrices are known.

In the channel estimation phase, the goal is to estimate $\boldsymbol{H}$ from $\boldsymbol{X}$. For this purpose it is desirable to design the analog combiner $\boldsymbol{W}_{RF}$ to minimize the MSE in estimation. As shown in [24], the estimation error of the MMSE estimator for $\boldsymbol{H}$ from $\boldsymbol{X}$ is inversely proportional to

$$\mu \triangleq \text{tr}\left(\boldsymbol{W}_{RF}^* \boldsymbol{R}_r^2 \boldsymbol{W}_{RF} \left(\boldsymbol{W}_{RF}^* \boldsymbol{R}_r \boldsymbol{W}_{RF}\right)^{-1}\right), \quad (40)$$

which is equal to (32) with $\boldsymbol{A} = \boldsymbol{R}_r^2$ and $\boldsymbol{B} = \boldsymbol{R}_r$. Hence, all the previously mentioned methods may be used to design $\boldsymbol{W}_{RF}$.

VI. NUMERICAL EXPERIMENTS

We now demonstrate the performance of the suggested beamformers under different hardware constraints. Unless mentioned otherwise, the channel model used is the narrow-band mmWave clustered channel defined in (26), with $\alpha_{il} \sim \mathcal{CN}(0,1)$, $N_{cl} = 6$, and $N_{ray} = 4$. We consider a simple uniform linear array (ULA) with spacing $d = \frac{\lambda}{2}$, where λ is the carrier wavelength. It follows that the steering vectors depend only on the azimuth and are given by

$$\boldsymbol{a}_q(\phi) = \frac{1}{\sqrt{N}}\left[1, e^{j2\pi \sin(\phi)}, \cdots, e^{j2\pi(N_q-1)\sin(\phi)}\right], \quad (41)$$

for $q \in \{r, t\}$. The angles ϕ_{il}^t, ϕ_{il}^r are distributed uniformly over the interval $[0, 2\pi)$.

Unless mentioned otherwise, the interference is a white complex-Gaussian noise with zero mean and variance $\sigma_z^2 = 1$. For the precoder experiments, we used a fully-digital receiver, i.e. $N_{RF}^r = N_r$, and for the combiner experiments we used a fully-digital transmitter, i.e. $N_{RF}^t = N_t$.

A. Hybrid Precoder Performance

First, we present the performance of different hybrid precoders. Here, we compare 5 design methods. The first two are the MO-AltMin algorithm from [11], which performs manifold optimization to minimize (15) over $\boldsymbol{F}_{RF}$ and $\boldsymbol{F}_{BB}$, and the PE-AltMin method, also from [11], that assumes $\boldsymbol{F}_{BB}$ to be a scaled orthogonal matrix and employs an algorithm similar to Algorithm 2, only with $\boldsymbol{F}_{BB}$ calculated in the last step as $\boldsymbol{F}_{BB} = \frac{\sqrt{N_S}}{\|\boldsymbol{F}_{RF}\boldsymbol{T}\|_F}\boldsymbol{T}$. The third is the SOMP of [4], that reformulates (15) as a sparsity problem and chooses the columns of $\boldsymbol{F}_{RF}$ from a dictionary of candidate vectors, and simultaneously solves the corresponding weights $\boldsymbol{F}_{BB}$. Last two are our methods, the MaGiQ in Algorithm 2 and the Alt-MaG method in Algorithm 1 with the MO-AltMin solution used to obtain $\boldsymbol{F}_{RF}, \boldsymbol{F}_{BB}$ in step 1. For the AltMin algorithms, we used the Matlab's functions in [27]. The dictionary used for the SOMP algorithm consists of 1000 steering vectors $\{\boldsymbol{a}_t(\frac{2\pi}{1000}q)\}_{q=1}^{1000}$. As performance measure we consider the gap between the estimation error of the optimal precoder (14) and the hybrid one,
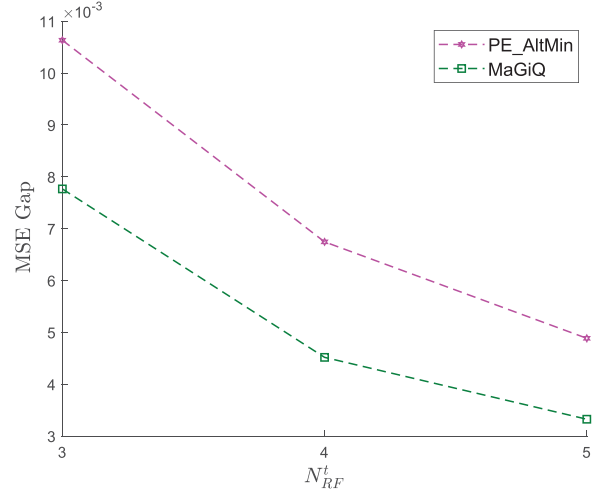

Fig. 2. Precoder estimation gap $\epsilon - \epsilon_{opt}$ vs. number of RF chains N_{RF}^t, for MAGiQ and PE-AltMin.
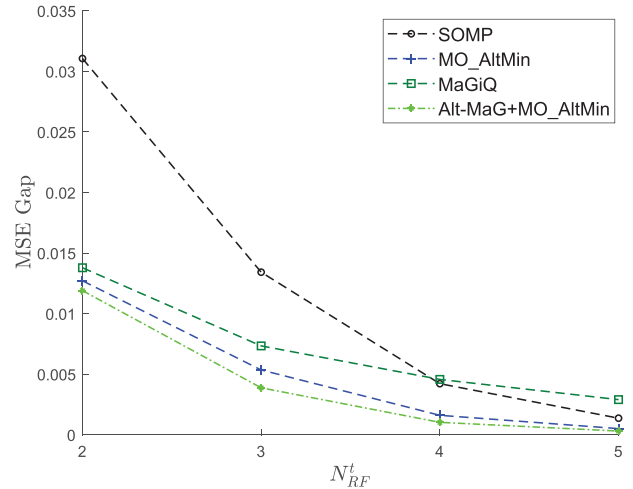

Fig. 3. Precoder estimation gap $\epsilon - \epsilon_{opt}$ vs. number of RF chains N_{RF}^t, for a fully-connected phase shifters network S2.

defined by $\epsilon - \epsilon_{opt}$ with $\epsilon = \frac{1}{N_s \cdot Q} \sum_{q=1}^Q \|\hat{\boldsymbol{s}} - \boldsymbol{s}\|^2$ and Q the number of realizations.

We begin by comparing MaGiQ and PE-AltMin considering a fully-connected phase shifters network S2. Here, the number of transmit antennas is $N_t = 10$ and the number of receive antennas is $N_r = 15$. As mentioned before, these two algorithms are very similar except for the last step of calculating $\boldsymbol{F}_{BB}$ which in PE-AltMin is set as $\boldsymbol{F}_{BB} = \frac{\sqrt{N_S}}{\|\boldsymbol{F}_{RF}\boldsymbol{T}\|_F}\boldsymbol{T}$, and in MaGiQ is calculated using (23). Fig. 2 demonstrates that the digital precoder of MAGiQ enjoys lower MSE. In the next simulations, PE-AltMin will not be tested.

Figure 3 presents the estimation gap with respect to the number of RF chains for the different design methods. Since the runtime of MO-AltMin increases with the number of antennas, we set here $N_t = 10$ and $N_r = 15$. The SOMP algorithm suffers from a large performance gap, especially when the number of RF chains is much smaller than the number of multipath components, i.e. $N_{RF}^t \ll N_c$. MaGiQ enjoys both low complexity
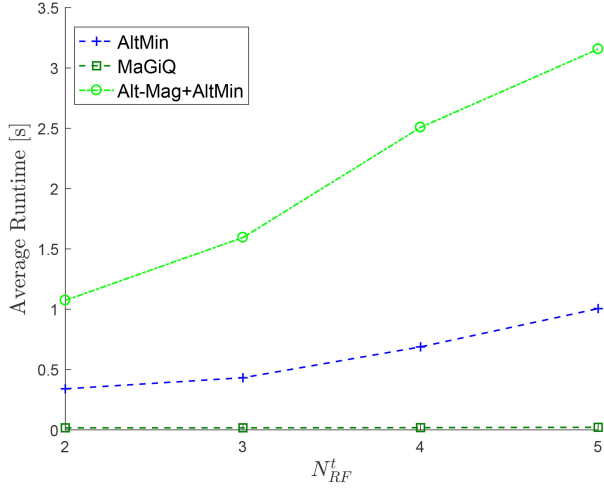
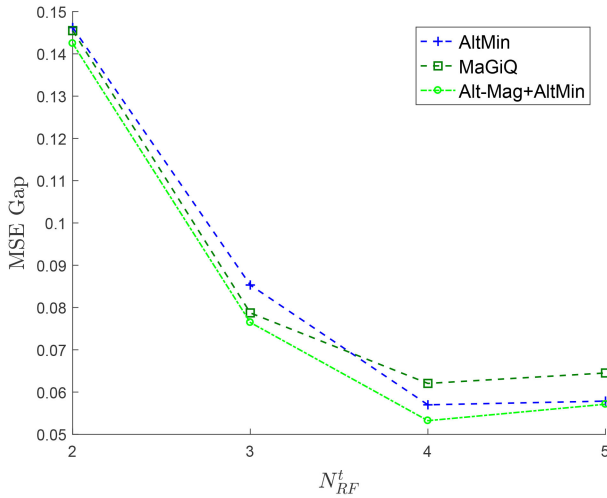Fig. 4. Algorithm runtime vs. number of RF chains N_{RF}^t, for a fully-connected phase shifters network S2.

Fig. 5. Precoder estimation gap $\epsilon - \epsilon_{opt}$ vs. number of RF chains N_{RF}^t, for a fully-connected phase shifters network S2.
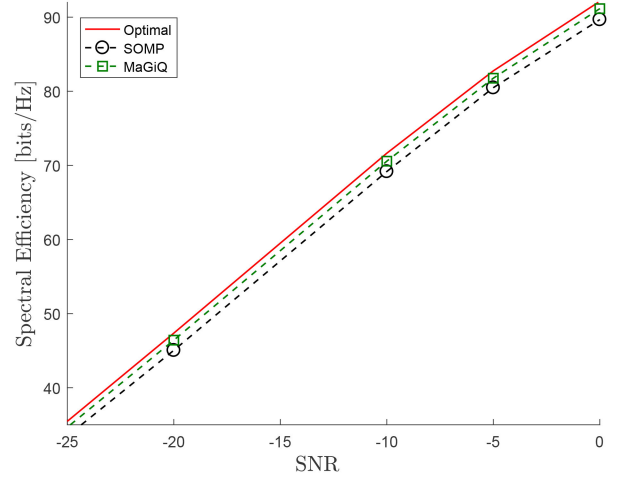

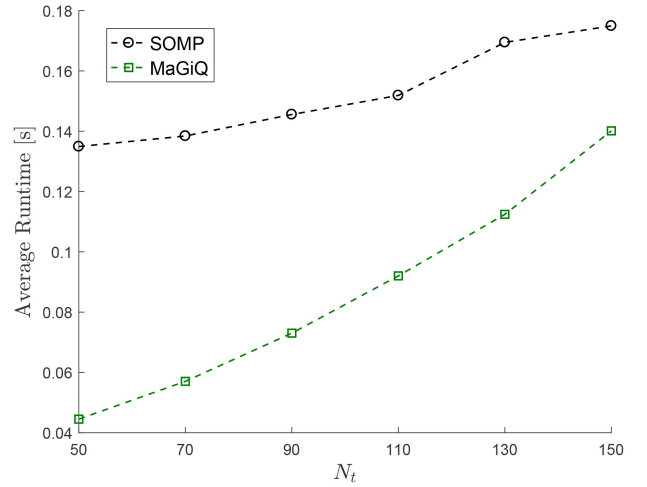Fig. 6. Spectral efficiency vs. SNR, for MAGiQ and SOMP precoders with $N_t = 128$ and $N_{RF}^t = 8$.

Fig. 7. Algorithm runtime vs. number of transmit antennas N_t, for MAGiQ and SOMP precoders with $N_{RF}^t = 8$ and SNR = 0[dB].

and good performance due to the alternating minimization over T in (16). The MO-AltMin algorithm achieves low MSE at the cost of long running time. The gap between Alt-MaG and MO-AltMin demonstrates the potential gain in optimizing over the matrix T in (16), in comparison to optimizing only over F_{RF}, F_{BB} as in (15).

The substantial improvement in performance with negligible increase in runtime is demonstrated in Fig. 4 which reports the run time of MO-AltMin, MaGiQ and AltMaG with MO-AltMIn, when $N_t = 25$ and $N_r = 30$. The corresponding MSE is presented in Fig. 5. It can be seen that AltMaG runtime is only 2-3 times the one of MO-AltMin, which implies that it requires approximately 3 iterations to converge. The short runtime of MAGiQ is also demonstrated here, as well as its low MSE when using very small number of RF chains. This emphasizes the strength of MAGiQ, which achieves similar and sometimes better performance than other algorithms, but has an order of magnitude shorter runtime. Moreover, MaGiQ's runtime

barely depends on the number of RF chains, unlike the other techniques, whose runtime grows with the number of chains.

Next, we consider the system's spectral efficiency as the performance criteria. In this case the optimal fully-digital solution is (14) with Φ now being a diagonal matrix with the power allocation weights given by water filling [17].

Figure 6 presents the spectral efficiency for different SNR values. Here $N_t = 128$ and $N_{RF}^t = 8$, that is, the number of RF chains is small compared to the number of transmit antennas. This is a reasonable assumption for massive MIMO systems. Due to the large number of antennas, in this scenario, only MAGiQ and SOMP were tested, as MO-AltMin suffers from a very long runtime in this regime. It can be seen that MaGiQ achieves approximately one additional bit per Hz above SOMP.

To further demonstrate the benefits of MAGiQ, we set a scenario with $N_{RF}^t = 8$ and investigate the runtime and spectral efficiency of MaGIQ and SOMP vs. the number of transmit antennas. In this scenario $N_{RF}^t \ll N_t$. In Figs. 7 and 8 we can see that for a very short runtime it offers several bits per Hz more than SOMP.
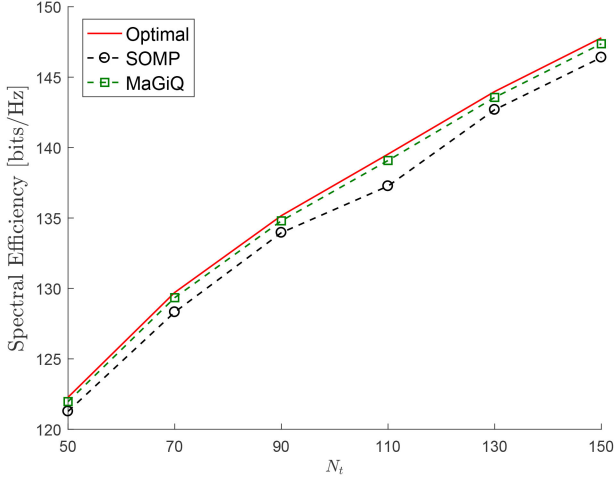
Fig. 8. Spectral efficiency vs. number of transmit antennas N_t, for MAGiQ and SOMP precoders with $N_{RF}^t = 8$ and SNR = 0[dB].
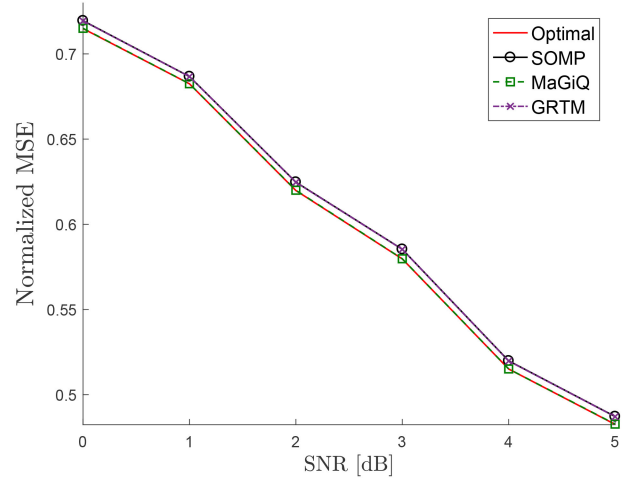

Fig. 10. Combiner estimation error vs. SNR for a fully-connected phase shifters network S2 and mmWave channel with asymptotic number of antennas.
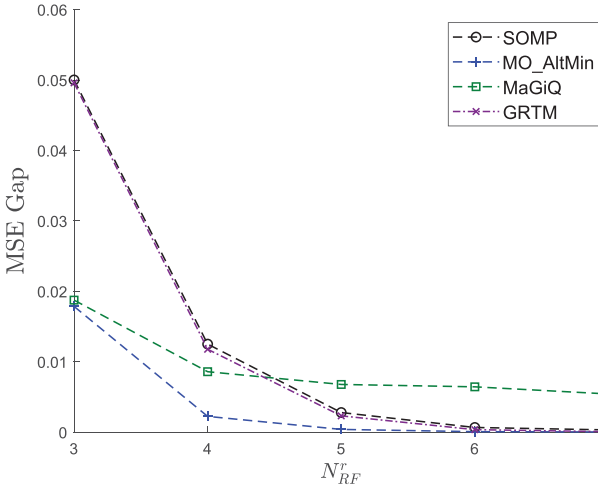

Fig. 9. Combiner estimation gap $\epsilon - \epsilon_{opt}$ vs. number of RF chains N_{RF}^r, for a fully-connected phase shifters network S2.
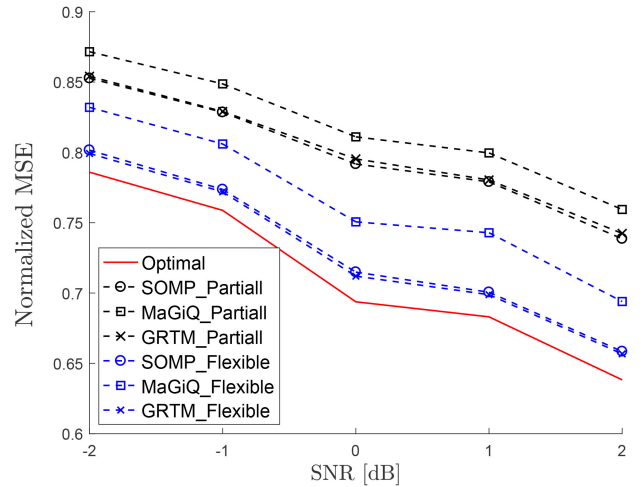

Fig. 11. Combiner estimation error vs. SNR for the partially connected phase shifters networks S4 and S5 with $G = 5$.

B. Hybrid Combiner Performance

We now investigate the combiner's performance. Here, an additional algorithm is tested, the GRTM of Algorithm 3, with the dictionary-based method in Section V-B as the base case solution. In contrast to the precoder case, here the SOMP algorithm solves the problem (30) as suggested in [4]. We set $N_t = 10$ and $N_r = 15$.

Figure 9 presents the estimation gap from the optimal combiner for all approaches with the fully-connected phase shifters scheme S2. It can be seen that MO-AltMin provides the best results. However, its runtime is an order-of-magnitude larger than the runtime of the other methods. Again, in the case of very few RF chains, MaGiQ is preferred over the greedy methods GRTM and SOMP, which suffer from large performance gap in that scenario. With additional RF chains, the greedy algorithms outperform the simple MaGiQ, with a slight advantage to GRTM.

Next, we show that in some special cases, MaGiQ coincides with the fully-digital solution and outperforms other methods. We demonstrate this using the scenario from the asymptotic example given in Section IV. Here, $\boldsymbol{H}$ is the mmWave channel (26), with $N_c = 4$, $N_{RF}^r = 4$, and $N_r = 150$. In this case, MO-AltMin cannot be used due to its long runtime that grows with the number of antennas. Since $N_c \ll N_r$ the asymptotic analysis holds, and $\boldsymbol{H}$ has unimodular singular vectors. Figure 10 shows the estimation error ϵ of the different algorithms. It can be seen that MaGiQ's performance coincides with the fully-digital combiner. We used a steering dictionary for both SOMP and GRTM. Since the singular vectors of the channel also have steering structure, the greedy methods performance gap is small, but still exists.

Next, we investigate the partially connected schemes. Figure 11 shows the performance of different combiners for the fixed sub-arrays network S4 and for the flexible one S5. For both scenarios, we set $G = 5$. We first notice the additional
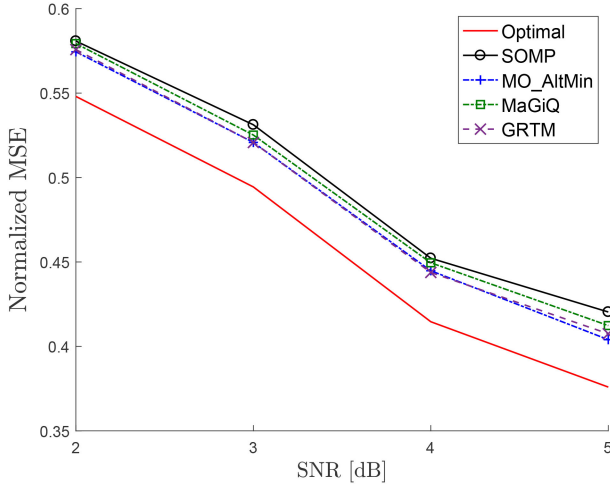
Fig. 12. Combiner estimation error vs. SNR for the fully-connected phase shifters and switches network S1 with general channel model and interference.

Fig. 13. Combiner estimation error vs. SNR for a partially connected phase shifters network S4 with $G = 3$.

performance gain of the flexible architecture. This result is natural since the additional switches allow each RF chain to choose the antennas that contribute to it, in contrast to the fixed sub-arrays case, that enforces each RF chain to be connected to a small predetermined array. In both scenarios, the greedy methods outperform MaGiQ, but while SOMP yields better performance for the fixed arrays, when adding switches to allow for flexibility, GRTM is preferred.

The fully-connected network S1, that involves switches as well as phase shifters is considered next. Here, we use a general channel model such that H has i.i.d complex-Gaussian entries and the interference z is now a complex-Gaussian vector with arbitrary full rank covariance matrix R_z. For the SOMP and GRTM algorithms, we used the dictionary $\bar{W} = P_{\mathcal{W}}(X)$, with $\mathcal{W}$ the feasible set for scheme S1, as explained in Section V-B. Figure 12 presents the MSE ϵ as a function of SNR. The complex MO-AltMin algorithm now achieves approximately the same performance as the low complexity GRTM. This is because MO-AltMin cannot use the additional flexibility of the switches and produces only unimodular beamformer vectors. This demonstrates a trade-off between hardware and computational complexity: one may use the simpler architecture S2 while achieving the same performance as the complex network S1, with the cost of using a heavy computational algorithm such as MO-AltMin. It can be further noticed that SOMP's performance falls short in comparison to others, possibly due to the different interference structure.

C. Hardware Schemes Comparison

The last simulation considers the different hardware choices. In Fig. 13, the performance of the MaGiQ combiner under different hardware constraints is demonstrated. As expected, the simple switching network S3 suffers from the largest MSE, as its connectivity is the most limited. The two partially connected cases S4 and S5 with $G = 5$ offer lower MSE, due to the additional hardware complexity, where the second performs better as a result of the additional switches. The two fully-connected
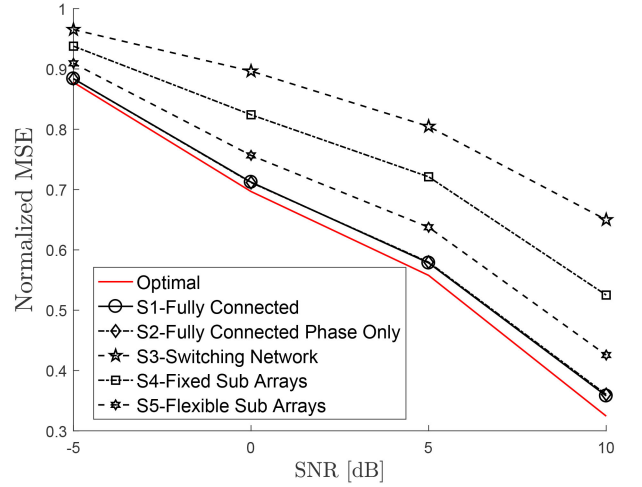
architectures S1 and S2 show similar performance, suggesting that the additional switches in the first offer negligible improvement. This surprising result can be explained by the channel model which implies that the optimal combiner consists of sums of steering vectors, which can be efficiently described using unimodular vectors.

VII. Conclusions

We developed a framework for hybrid precoder and combiner design, applicable to various channel models and hardware settings. Our framework is suitable for massive MIMO systems and as such can fit 5G cellular networks. We considered a data estimation problem and aimed at minimizing the estimation MSE over all possible hybrid precoders/combiners. For the precoder side, we suggested a family of iterative algorithms, Alt-MaG, that approximates the optimal fully-digital precoder while seeking the solution in the optimal set that results in the smallest approximation gap from the hybrid precoder of the previous iteration. The potential gain in exploiting the unitary degree of freedom in the fully-digital precoder was demonstrated in simulations. We further suggested a simple low complexity algorithm, MaGiQ, that achieves good approximation using a simple quantization function, and yields better performance than other methods suggested in the literature. We also showed that in some special cases it coincides with the optimal fully-digital solution.

Next, we adjusted the MaGiQ algorithm so that it can be used for combiner design. We then suggested an additional greedy algorithm, GRTM, that directly minimizes the MSE using a simple scalar-ratio objective at each iteration. GRTM achieves lower MSE than MaGiQ when the number of RF chains increases. Experimental results showed that our low-complexity algorithms enjoy good performance in various scenarios.

Finally, using simulations, we showed that in partially connected schemes and sparse multipath mmWave channels, adding switches to the analog network offers a large increase in performance, while in fully-connected cases the improvement is negligible.

REFERENCES

[1] J. G. Andrews *et al.*, "What will 5G be?" *IEEE J. Sel. Areas Commun.*, vol. 32, no. 6, pp. 1065–1082, Jun. 2014.

[2] F. Rusek, D. Persson, Buon Kiong Lau, E. G. Larsson, T. L. Marzetta, and F. Tufvesson, "Scaling up MIMO: Opportunities and challenges with very large arrays," *IEEE Signal Process. Mag.*, vol. 30, no. 1, pp. 40–60, Jan. 2013.

[3] T. S. Rappaport *et al.* "Millimeter wave mobile communications for 5G cellular: It will work!," *IEEE Access*, vol. 1, pp. 335–349, 2013.

[4] O. E. Ayach, S. Rajagopal, S. Abu-Surra, Z. Pi, and R. W. Heath, "Spatially sparse precoding in millimeter wave MIMO systems," *IEEE Trans. Wireless Commun.*, vol. 13, no. 3, pp. 1499–1513, Mar. 2014.

[5] F. Sohrabi and W. Yu, "Hybrid digital and analog beamforming design for large-scale antenna arrays," *IEEE J. Sel. Topics Signal Process.*, vol. 10, no. 3, pp. 501–513, Apr. 2016.

[6] A. Alkhateeb, O. El Ayach, G. Leus, and R. W. Heath, "Hybrid precoding for millimeter wave cellular systems with partial channel knowledge," in *Proc. IEEE Inf. Theory Appl. Workshop*, Feb. 2013, pp. 1–5.

[7] Y.-Y. Lee, C.-H. Wang, and Y.-H. Huang, "A hybrid RF/baseband precoding processor based on parallel-index-selection matrix-inversion-bypass simultaneous orthogonal matching pursuit for millimeter wave MIMO systems," *IEEE Trans. Signal Process.*, vol. 63, no. 2, pp. 305–317, Jan. 2015.

[8] R. Mendez-Rial, C. Rusu, N. Gonzalez-Prelcic, A. Alkhateeb, and R. W. Heath, "Hybrid MIMO architectures for millimeter wave communications: Phase shifters or switches?" *IEEE Access*, vol. 4, pp. 247–267, 2016.

[9] M. Kim and Y. H. Lee, "MSE-based hybrid RF/baseband processing for millimeter-wave communication systems in MIMO interference channels," *IEEE Trans. Veh. Technol.*, vol. 64, no. 6, pp. 2714–2720, Jun. 2015.

[10] S. Payami, M. Ghoraishi, and M. Dianati, "Hybrid beamforming for large antenna arrays with phase shifter selection," *IEEE Trans. Wireless Commun.*, vol. 15, no. 11, pp. 7258–7271, Nov. 2016. [Online]. Available: http://ieeexplore.ieee.org/document/7542170/

[11] X. Yu, J.-C. Shen, J. Zhang, and K. B. Letaief, "Alternating minimization algorithms for hybrid precoding in millimeter wave MIMO systems," *IEEE J. Sel. Topics Signal Process.*, vol. 10, no. 3, pp. 485–500, Apr. 2016.

[12] J. Singh and S. Ramakrishna, "On the feasibility of codebook-based beamforming in millimeter wave systems with multiple antenna arrays," *IEEE Trans. Wireless Commun.*, vol. 14, no. 5, pp. 2670–2683, May 2015.

[13] X. Yu, J. Zhang, and K. B. Letaief, "Partially-connected hybrid precoding in mm-Wave systems with dynamic phase shifter networks," in *Proc. IEEE 18th Int. Workshop Signal Process. Adv. Wireless Commun.*, 2017, pp. 1–5.

[14] S. Park, A. Alkhateeb, and R. W. Heath, "Dynamic subarrays for hybrid precoding in wideband mmWave MIMO systems," *IEEE Trans. Wireless Commun.*, vol. 16, no. 5, pp. 2907–2920, May 2017.

[15] S. Han, I. Chih-Lin, Z. Xu, and C. Rowell, "Large-scale antenna systems with hybrid analog and digital beamforming for millimeter wave 5G," *IEEE Commun. Mag.*, vol. 53, no. 1, pp. 186–194, Jan. 2015.

[16] Y. C. Eldar and G. Kutyniok, *Compressed Sensing: Theory and Applications.* Cambridge, U.K.: Cambridge Univ. Press, 2012.

[17] A. Scaglione, P. Stoica, S. Barbarossa, G. Giannakis, and H. Sampath, "Optimal designs for space-time linear precoders and decoders," *IEEE Trans. Signal Process.*, vol. 50, no. 5, pp. 1051–1064, May 2002.

[18] S. X. Yu and J. Shi, "Multiclass spectral clustering," in *Proc. Int. Conf. Comput. Vision.*, Oct. 2003, pp. 313–319.

[19] A. Sayeed, "Deconstructing multiantenna fading channels," *IEEE Trans. Signal Process.*, vol. 50, no. 10, pp. 2563–2579, Oct. 2002.

[20] P. F. M. Smulders and L. M. Correia, "Characterisation of propagation in 60 GHz radio channels," *Electron. Commun. Eng. J.*, vol. 9, no. 2, pp. 73–80, 1997.

[21] H. Xu, V. Kukshya, and T. S. Rappaport, "Spatial and temporal characteristics of 60-GHz indoor channels," *IEEE J. Sel. Areas Commun.*, vol. 20, no. 3, pp. 620–630, Apr. 2002.

[22] K. B. Petersen and M. S. Pedersen, "The matrix cookbook," Lyngby, Denmark: Tech. Univ. Denmark, Nov. 2012. [Online]. Available: http://localhost/pubdb/p.php?3274

[23] H. Wang, S. Yan, D. Xu, X. Tang, and T. Huang, "Trace ratio vs. ratio trace for dimensionality reduction," in *Proc. IEEE Conf. Comput. Vision Pattern Recognit.*, 2007, pp. 1–8.

[24] S. S. Ioushua and Y. C. Eldar, "Pilot contamination mitigation with reduced RF chains," *Signal Process. Adv. Wireless Commun.*, Jul. 2017, pp. 1–5.

[25] E. Bjornson and B. Ottersten, "A framework for training-based estimation in arbitrarily correlated Rician MIMO channels with Rician disturbance," *IEEE Trans. Signal Process.*, vol. 58, no. 3, pp. 1807–1820, Mar. 2010.

[26] A. Tulino, A. Lozano, and S. Verdu, "Impact of antenna correlation on the capacity of multiantenna channels," *IEEE Trans. Inf. Theory*, vol. 51, no. 7, pp. 2491–2509, Jul. 2005.

[27] N. Boumal, B. Mishra, P. Absil, and R. Sepulchre, "Manopt, a MATLAB toolbox for optimization on manifolds," *J. Mach. Learn. Res.*, vol. 15, pp. 1455–1459, Jan. 2014.

Shahar Stein Ioushua (S'15) received the B.Sc. degree in electrical engineering (*cum laude*) in 2015 and the M.Sc. degree in electrical engineering (*cum laude*) in 2018, both from the Technion—Israel Institute of Technology (Technion), Haifa, Israel. She is currently working toward the Ph.D. degree in electrical engineering in Tel Aviv University, Tel Aviv, Israel.

From 2015 to 2018, she was a Teaching Assistant with the Viterbi Faculty of Electrical Engineering and a Project Supervisor with the Signal Acquisition, Modeling and Processing Lab, Electrical Engineering Department, Technion. She is a co-founder of the WomEE forum for women in graduate studies in the Electrical Engineering Department, Technion. Her research interests include information theory, data compression, theoretical aspects of signal processing, compressed sensing, and signal processing for communication signals.

Mrs. Stein Ioushua received the Meyer Foundation Excellence prize in 2015. She has been an Gutwirth Fellow since 2017.

Yonina C. Eldar (S'98–M'02–SM'07–F'12) received the B.Sc. degree in physics in 1995 and the B.Sc. degree in electrical engineering in 1996 both from Tel Aviv University, Tel Aviv, Israel, and the Ph.D. degree in electrical engineering and computer science in 2002 from the Massachusetts Institute of Technology (MIT), Cambridge, MA, USA.

She is currently a Professor with the Department of Mathematics and Computer Science, Weizmann Institute of Science, Rehovot, Israel. She was previously a Professor with the Department of Electrical Engineering, Technion, where she held the Edwards Chair in Engineering. She is also a Visiting Professor at MIT, a Visiting Scientist at the Broad Institute, and an Adjunct Professor at Duke University, and was a Visiting Professor at Stanford. Her research interests are in the broad areas of statistical signal processing, sampling theory and compressed sensing, learning and optimization methods, and their applications to biology and optics.

Dr. Eldar is a member of the Israel Academy of Sciences and Humanities (elected 2017) and a EURASIP Fellow. She has received numerous awards for excellence in research and teaching, including the IEEE Signal Processing Society Technical Achievement Award (2013), the IEEE/AESS Fred Nathanson Memorial Radar Award (2014), and the IEEE Kiyo Tomiyasu Award (2016). She was a Horev Fellow of the Leaders in Science and Technology program at the Technion and an Alon Fellow. She received the Michael Bruno Memorial Award from the Rothschild Foundation, the Weizmann Prize for Exact Sciences, the Wolf Foundation Krill Prize for Excellence in Scientific Research, the Henry Taub Prize for Excellence in Research (twice), the Hershel Rich Innovation Award (three times), the Award for Women with Distinguished Contributions, the Andre and Bella Meyer Lectureship, the Career Development Chair at the Technion, the Muriel & David Jacknow Award for Excellence in Teaching, and the Technion's Award for Excellence in Teaching (twice). She received several best paper awards and best demo awards together with her research students and colleagues including the SIAM outstanding Paper Prize and the IET Circuits, Devices and Systems Premium Award, and was selected as one of the 50 most influential women in Israel.

She was a member of the Young Israel Academy of Science and Humanities and the Israel Committee for Higher Education. She is the Editor-in-Chief of Foundations and Trends in Signal Processing, a member of the IEEE Sensor Array and Multichannel Technical Committee, and serves on several other IEEE committees. In the past, she was a Signal Processing Society Distinguished Lecturer, member of the IEEE Signal Processing Theory and Methods and Bio Imaging Signal Processing technical committees, and served as an Associate Editor for the IEEE TRANSACTIONS ON SIGNAL PROCESSING, the *EURASIP Journal of Signal Processing*, the *SIAM Journal on Matrix Analysis and Applications*, and the *SIAM Journal on Imaging Sciences*. She was Co-Chair and Technical Co-Chair of several international conferences and workshops.